

Highly Nonlinear Dynamics of *In Vivo* Deep-Tissue Interaction with Femtosecond Laser Pulses at 1030 nm

Soyeon Jun^{1,2,4}, Andreas Herbst^{1,2}, Kilian Scheffter^{1,2}, Nora John^{1,3,5}, Julia Kolb^{1,3,5}, Daniel Wehner^{1,3,*}, Hanieh Fattahi^{1,2,*}

1. Max Planck Institute for the Science of Light, 91058 Erlangen, Germany

2. Friedrich-Alexander University Erlangen-Nürnberg, 91085 Erlangen, Germany

3. Max-Planck-Zentrum für Physik und Medizin, 91058 Erlangen, Germany

4. Friedrich-Alexander-Universität Erlangen-Nürnberg (FAU), Erlangen Graduate School in Advanced Optical Technologies (SAOT), 91052 Erlangen, Germany

5. Department of Biology, Animal Physiology, Friedrich-Alexander-University Erlangen-Nürnberg, 91058 Erlangen, Germany

* Correspondence: hanieh.fattahi@mpl.mpg.de, daniel.wehner@mpl.mpg.de

Abstract

We report on the highly nonlinear behavior observed in the central nervous system tissue of zebrafish (*Danio rerio*) when exposed to femtosecond pulses at 1030 nm. At this irradiation wavelength, photo damage becomes detectable only after exceeding a specific peak intensity threshold, which is independent of the photon flux and irradiation time, distinguishing it from irradiation at shorter wavelengths. Furthermore, we investigate and quantify the role of excessive heat in reducing the damage threshold, particularly during high-repetition-rate operations, which are desirable for label-free and multi-dimensional microscopy techniques. To verify our findings, we examined cellular responses to tissue damage, including apoptosis and the recruitment of macrophages and fibroblasts at different time points post-irradiation. These findings substantially contribute to advancing the emerging nonlinear optical microscopy techniques and provide a strategy for inducing deep-tissue, precise and localized injuries using near-infrared femtosecond laser pulses.

Keywords: photo damage, phototoxicity, photothermal damage, reactive oxygen species, zebrafish, deep-tissue imaging, femtosecond pulses, light tissue interaction, central nervous system

Introduction

Light microscopy has revolutionized our ability to observe and understand biological processes. However, does the use of light perturb biological processes or induce pro-apoptotic fates? What is the most accurate definition of biological damage caused by our observation? Is it the instantaneous apoptosis of irradiated cells, as noted by [1], that constitutes damage? Or should any recoverable cellular impairment in a living organism already be classified as damage [2]? What if the illumination causes cell apoptosis by slowing down vital metabolic processes through the degradation of endogenous organic compounds [3]?

Life on Earth depends on light and is adapted to the solar flux of less than 1.4 kW/m^2 . It has been argued that this value should be used as a safe irradiance reference when observing dynamic biological processes [4]. However, the sun is a continuous source of incoherent radiation with a non-uniform multi-octave spectral coverage. While the organisms are adapted to harvest the energy of frequencies with the higher spectral density of the sun for their development through photosynthesis, they stayed ignorant of other lower spectral density components present in the solar spectrum [5]. Furthermore, the photo damage effect of continuous light on biological specimens differs from the effect of pulsed lasers at similar photon flux [6–8]. Therefore, it is crucial to carefully consider these factors when studying living organisms using light microscopy techniques. In the past few decades, two major types of microscopy have gained widespread usage: fluorescence microscopy, which utilizes the emission of linearly or non-linearly excited fluorophores to capture microscopic images of the sample [9–14]; and label-free microscopy, which relies on the emission of the molecular composition of the sample caused by an induced nonlinear polarization at high laser peak intensities [15–23]. Despite the distinct imaging methodologies utilized in these two categories, they share a common mechanism for causing photo damage.

When pulsed laser interacts with tissue, the molecules in the sample get excited to a higher energy state through single-photon or multiphoton absorption, depending on the illumination peak intensity and optical frequency. The molecules can then transition back to the ground state either non-radiatively, which can lead to thermal damage, or via de-excitation processes. De-excitation involves dissociation or changes in the redox state of the absorbing molecule, energy transfer to a dioxygen molecule, or formation of reactive oxygen species (ROS), resulting in localized chemical perturbations and cell death [24–27]. At extremely high peak intensities, ionization of molecules and formation of a low-density plasma takes place, leading to photochemical damage and production of supersonic shock waves, which likewise lead to tissue damage [28–31]. In both of these categories of microscopy, the interaction between the laser pulses and tissue involves absorbers, predominantly consisting of fluorescence labels in

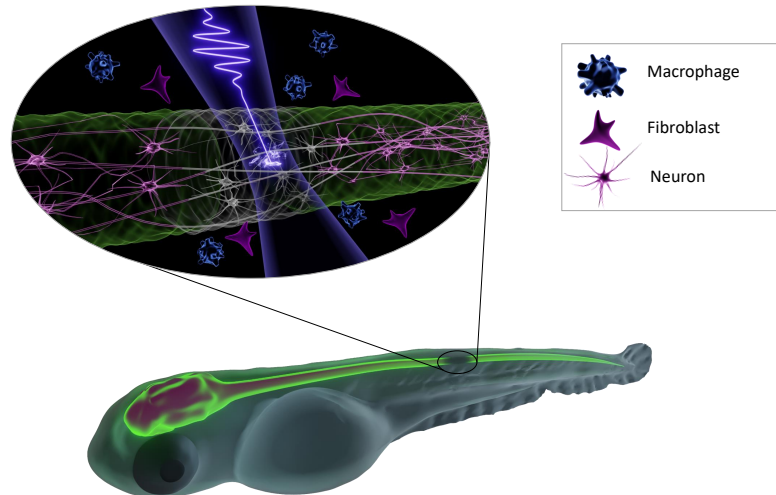


Figure 1: Graphical Abstract of the Experiment: To investigate the in-vivo interaction of femtosecond pulses within deep-tissues, zebrafish larvae served as our model organism. Precisely targeted femtosecond laser pulses were focused on the central nervous system (CNS) of the zebrafish under various irradiation settings. The cellular dynamics resulting from this pulse-tissue interaction were meticulously observed over time, focusing on neuronal cells and gauging the responsiveness of macrophages and fibroblasts.

fluorescence microscopy [32, 33]; and water molecules [34] or other tissue components depending on the excitation wavelength [35–39] in label-free microscopy. While ROS generation has a significant impact on cell damage in fluorescence microscopy, its contribution in label-free microscopy is negligible. Therefore, there has been significant attention on using different label-free microscopy techniques in recent years [16, 40–44]. Moreover, due to its large penetration depth and image contrast, label-free microscopy has become a crucial tool for deep-tissue imaging [11, 45–50]. The complementary information provided by both categories of microscopy has led to the development of more advanced techniques, such as multimodal nonlinear microscopy [51–55].

Over the last decades, a significant body of research has been conducted on the effects of short laser pulses on thin *in vitro* samples in nonlinear fluorescence microscopy [1, 19, 56–59]. Despite these numerous investigations, a comprehensive study on how laser irradiation affects cell viability in a deep-tissue imaging setting, specifically for label-free and multimodal nonlinear microscopy, has not been fully explored. This study leverages the vertebrate species zebrafish (*Danio rerio*) to delve into the mechanisms of photo damage in deep-tissue at a cellular level, triggered by femtosecond excitation pulses. Our objectives revolve around elucidating several key questions: How do the dynamics of different photo damage mechanisms unfold across a spectrum of irradiation wavelengths? Is it feasible to reach plasma formation without inducing gradual damage to the sample due to thermal effects and chemical reactions? How does the repetition rate of laser pulses impact the photo damage threshold? While our study confirms that the severity of photo damage at shorter wavelengths is proportional to the illumination photon flux, we demonstrate the nonlinear scaling of *in vivo* photo damage in native vertebrate tissue when irradiated by near-infrared femtosecond pulses. We have found that in this particular regime and in the absence of a direct excitation path, it is possible to extend the irradiation time, therefore photon flux, extensively and noninvasively, as long as the irradiation peak intensity does not surpass the peak intensity damage threshold.

Results

Evaluating *in vivo* phototoxicity in deep-tissues is considerably more intricate than in cultured cells, where the use of probes for ROS production or observation of cell death through carbonization are common. In this study, we used the vertebrate species zebrafish at three days post-fertilization (dpf) to investigate interactions between femtosecond pulses and deep-tissues in a living organism. To assess photo damage levels of the spinal cord and surrounding trunk tissue, we employed two complementary criteria. Short-term damage was evaluated by monitoring the immediate physiological response, that is loss of tissue integrity, at the whole tissue level as well as of specific fluorescently labeled cell types. Long-term damage was assessed by observing spinal cord regeneration, histological stains to detect cell death, and injury-associated recruitment of reactive fibroblasts and immune cells within 24 hours post-irradiation (hpi) [60, 61].

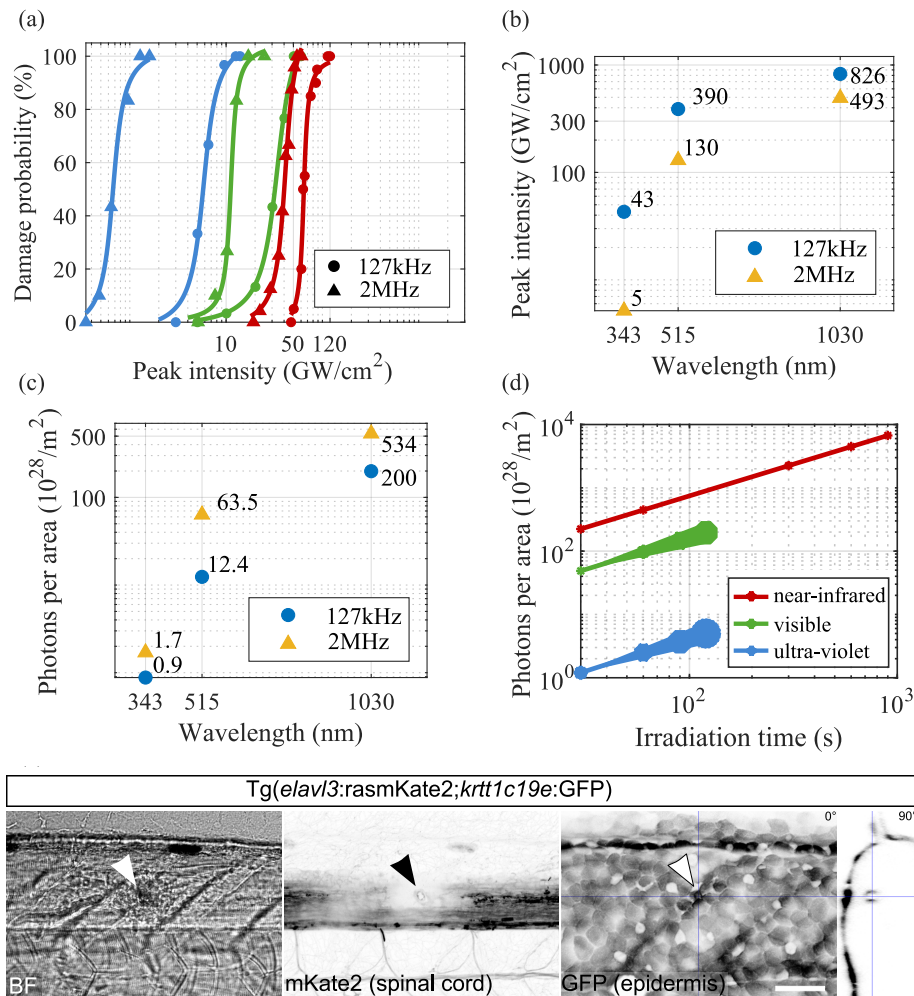


Figure 2: a) The damage probability of zebrafish spinal cord versus peak intensity of 250 fs pulses at various irradiation wavelengths and laser repetition rates. Irradiation at 343 nm, 515 nm, and 1030 nm are represented by blue, green, and red curves, respectively. The circle indicates irradiation at 127 kHz repetition rates, while the triangle shows irradiation at 2 MHz repetition rates. b) The average values of the peak intensity threshold at various wavelengths and laser repetition rates. c) The comparison of the average photons per area threshold for different parameters. Irradiation time was fixed to 30 s. d) The damage of the spinal cord is observed when the samples were irradiated at 343 nm and 515 nm below the peak intensity damage threshold and at longer irradiation times of 30 s and 60 s respectively. For below-threshold irradiation at 1030 nm, no damage was observed by increasing the irradiation beyond 900 s. The thickness of the curves for 343 nm and 515 nm illustrates the severity of the damage qualitatively (see supplementary material). e) Trunk of a transgenic zebrafish larva with fluorescently labeled spinal cord (neurons; mKate2) and epidermis (basal keratinocytes; GFP) after 30 s irradiation with 1030 nm pulses above the damage threshold. Arrowheads indicate the focus of irradiation. While damage is visible at the level of the spinal cord, the superficially-located epidermis remained intact. Images shown are bright-field (BF) recordings and orthogonal projections of the confocal image (xy or yz view). Scale bar: 50 μm

Figure 1 presents a visual summary of the experiments conducted to investigate the damage mechanism upon the *in vivo*, deep-tissue interaction of femtosecond laser pulses with a zebrafish larva. To generate the required femtosecond laser pulses at various wavelengths for this study, the output of an ytterbium amplifier delivering 250 fs pulses at 1030 nm was up-converted to 515 nm and 343 nm through second- and third-harmonic generation, respectively. A Pockels cell was utilized for pulse picking and reducing the laser pulse train's repetition rate from 2 MHz to 127 kHz, enabling the differentiation of thermal damage contributions across various irradiation regimes. The generated femtosecond laser pulses were focused on the spinal cord using a reflective microscope objective. An imaging system was developed to monitor and adjust the focus position across different sections of the zebrafish. To monitor tissue damage at the different irradiation paradigms, we employed transgenic fluorescence reporter zebrafish lines labeling glial cells, neurons, epidermal cells, or macrophages to examine the photo damage at the skin and spinal cord. Damage was defined as the absence of fluorescence in the region of interest.

Two series of measurements were conducted to differentiate photo damage originating from linear processes, such as one-photon absorption and thermal damage (which should scale linearly with irradiation time and photon flux), from nonlinear processes triggered by laser peak intensity. In the first set of measurements, samples were exposed to varying peak intensities, while maintaining fixed irradiation times. In the second series, laser pulses with varying irradiation times and tissue at constant pulse energy were examined (note that below the damage threshold values determined from the first series). Additionally, these measurements were carried out at two distinct repetition rates to further discern the underlying photo damage processes.

In the first series of measurements, in total 180 zebrafish larvae were irradiated for 30 seconds at various peak intensities, repetition rates, and irradiation wavelengths. Figure 2 a) displays the spinal cord damage probability versus peak intensity, while Figure 2 b) presents the average damage intensity threshold for different parameters. Our study reveals a 50 times higher damage threshold for laser pulses at 1030 nm compared to those at 343 nm. Furthermore, irradiation at a lower repetition rate across all wavelengths leads to a higher damage threshold than irradiation at higher repetition rates within the same irradiation time, highlighting the impact of thermal damage. It has been observed that the damage behavior for the 1030 nm irradiation has a completely different qualitative behavior compared to 515 nm and 343 nm. As the peak intensity increases for the two shorter irradiation wavelengths, the lesion's dimension expands. However, for the 1030 nm wavelength, damage occurs abruptly, leading to the immediate generation of visible mechanical shockwaves (see Supplementary Information video).

Figure 2 c) summarizes the photons per area related to two irradiation regimes. Although ROS production is anticipated to be higher at 343 nm irradiation due to the linear absorption of the fluorophores GFP and mKate2 labeling neurons and glial cells, our results show that higher peak intensities can be achieved on the sample with lower photon flux. This finding is of critical importance, as ultra-violet pulses have generally been avoided for biological imaging due to their high phototoxicity and absorption by DNA [59, 62, 63].

In the second series of measurements, the irradiation time was increased while maintaining the peak intensity below the damage threshold. Our study on photon flux revealed that, for irradiation at 343 nm and 515 nm, the lesion expands with increased irradiation time, showing gradual damage. However, the response is entirely different for 1030 nm irradiation. By increasing the irradiation time at a peak intensity below the damage threshold, no damage was observed. Figure 2 d) shows photon flux versus irradiation time for three different wavelengths. At 343 nm, photo damage is visible following 30 s of irradiation, signifying that tissue damage at this wavelength is predominantly driven by linear mechanisms. In contrast, at 515 nm irradiation wavelength, damage was observed at double the photon flux threshold, hinting at the involvement of nonlinear processes. Remarkably, at 1030 nm, it is possible to extend the irradiation duration to several minutes, by keeping the peak intensity below the damage threshold.

For the samples deemed healthy in the first series of the experiment, we examined photo damage on the skin, using transgenic zebrafish with fluorescently labeled basal keratinocytes of the bilayered epidermis. Figure 2 e) depicts the bright-field, GFP-labeled basal keratinocytes and mKate2-labeled neurons following irradiation above the damage intensity threshold at 1030 nm. We observed a sharply declined fluorescence of the neuronal marker but not epidermal marker after irradiation, indicating that tissue damage was limited to deep-tissue levels. Similar results are observed for irradiation at the other two wavelengths, where no apparent damage was detected on the epidermis. To exclude the possibility that the reduction of fluorescence signal is a consequence of bleaching of the fluorophore and not due to tissue damage, we reassessed the animals at 24 hpi and 48 hpi. This showed an imperfect fluorescence pattern of the white matter tracts, supporting the regrowth of irradiation-damaged axonal fibers rather than recovery of fluorescence (Figure 3 a). To provide further evidence for tissue damage or its absence in the respective conditions, we assessed apoptosis by TUNEL assay and monitored the recruitment of immune cells and fibroblasts (Figure 3 b-d) to the irradiated site [60, 61]. Consistent with tissue damage, we observed the emergence of TUNEL⁺ cells as well as the recruitment of reactive fibroblasts (visualized with *pdgfrb*:GFP transgenic animals) and macrophages (visualized with *mpeg1*:mCherry transgenic animals) in samples irradiated at 1030 nm for 30 s above the damage threshold. In contrast, for samples irradiated below the damage threshold,

we did not observe TUNEL⁺, fibroblasts, or macrophages accumulating at the irradiation site. This supports our observation of nonlinear scaling of the damage at near-infrared and the absence of any gradual damage at this wavelength.

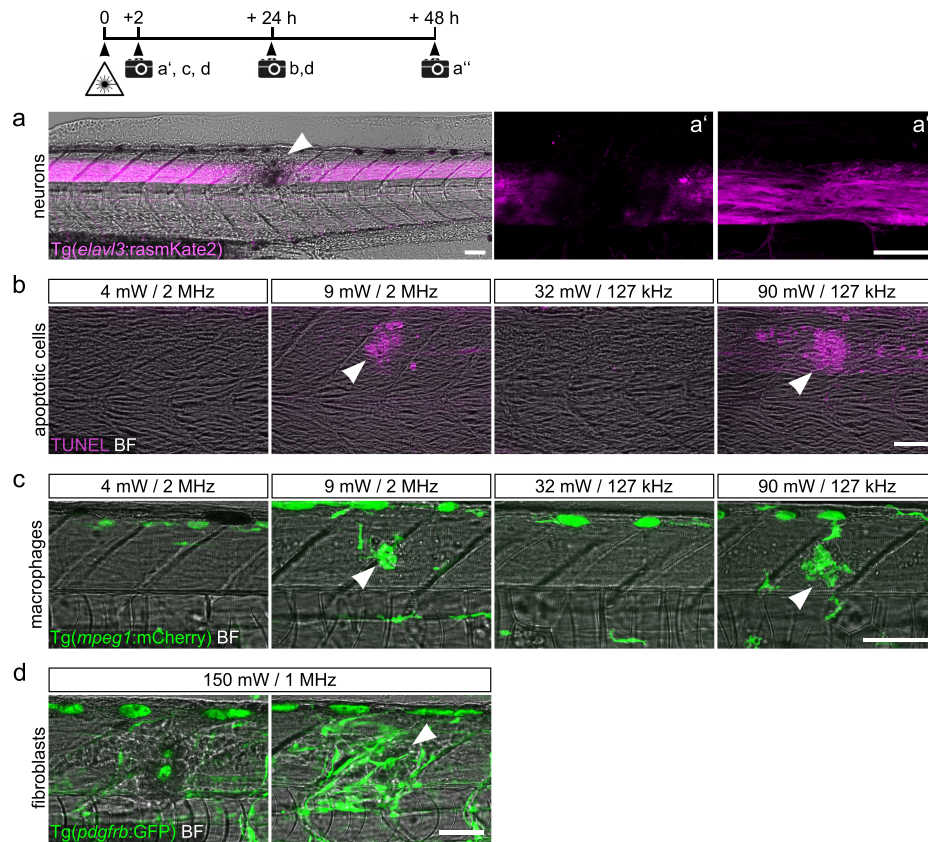


Figure 3: Cellular responses to different irradiation paradigms below and above the damage threshold. Timeline of experiments is indicated at the top. a) Spinal cord lesion induced by 300 mW pulses at 2 MHz (arrowhead in overview). The same animal is shown at 2 hpi (*a'*) and 48 hpi (*a''*). Note regrowth of white matter tracts at 48 hpi. b) Cell death (arrowheads), as detected by the TUNEL assay, is observed in the site of irradiation at above-damage threshold peak intensities. c) Recruitment of macrophages (arrowheads) to the irradiation site is observed at 9 mW at 2 MHz and 90 mW at 127 kHz however not at below damage threshold irradiations at the average powers of 4 mW at 2 MHz and 32 mW at 127 kHz. d) Irradiation at above damage threshold intensity leads to the accumulation of reactive fibroblasts in the irradiation site (arrowhead). Scale bars: 50 μ m.

Discussion

For successful implementation of cutting-edge nonlinear microscopy techniques for deep-tissue, *in-vivo* imaging and designing their use for medical applications, a comprehensive understanding of the non-invasive, optimal operational parameters and constraints of the imaging system is essential. This entails fine-tuning variables like the average power, peak intensity, wavelength, and pulse duration of the laser pulses, alongside other factors such as imaging irradiation time or dwell time. In addition, a rigorous assessment of thermal or photon-based damage mechanisms across various irradiation wavelengths is required. Equally important is the distinction between the impact of peak intensity, average power, and dwell time in nonlinear microscopy, as the nonlinear signal scales with peak intensity, while the signal-to-noise ratio is proportional to the average power of the laser pulse and dwell time. These parameters, though interconnected, may initiate various photo damage mechanisms and calls for a systematic and comprehensive study of these parameters for deep-tissue imaging.

Water, a major component of biological systems, exhibits five main resonances in the near-infrared at 0.76 μ m, 0.97 μ m, 1.19 μ m, 1.45 μ m, and 1.94 μ m, with an absorption cross section increasing by an order of magnitude when scaling between the adjunct resonances [64]. With recent advancements in ytterbium lasers operating at

1030 nm [65], alongside the advancement of novel detection schemes [66], the second near-infrared window of the tissue has become an increasingly fitting candidate for label-free nonlinear imaging [67, 68].

In this study, we reported on an exceptionally higher photo damage threshold for skin and central nervous system (CNS) tissue of zebrafish when irradiated by femtosecond pulses at 1030 nm compared to irradiation at shorter wavelengths. Our data provide hints on the mechanisms of photo damage in deep-tissue when using pulsed near-infrared excitation pulses. We demonstrate that when samples are subjected to ultra-violet and visible light irradiation, the extent of the photo damage is gradual and scales proportional to irradiation photon flux. In contrast, for irradiation at 1030 nm, the damage appears abruptly, leading directly to ablation. It is well understood that the ablation threshold is lower for shorter wavelengths due to the more efficient photoionization [28]. However, in our study, the gradual linear damage at shorter wavelengths, owing to linear absorption, prevents the irradiated samples to reach the ablation regime. When it comes to ablation with near-infrared irradiation, collisional absorption stands out as the primary mechanism for energy deposition. We report the observation of ablation triggered by near-infrared pulses at an average fluence of 4.4 J/cm² at 2 MHz operation and at the average fluence of 6.4 J/cm² for 127 kHz operation. Ablation severity escalates at a higher repetition rate due to the generation of a thermal shock wave (see Supplementary Information videos). This supports the assertion that one-photon absorption by water in the second near-infrared window of tissue does not significantly impact the near-infrared excitation process and the damage process is highly nonlinear.

When conducting *in vivo* deep-tissue nonlinear microscopy, it is crucial to evaluate various photo damage mechanisms collectively, since they operate in unison at differing intensities upon the interaction of femtosecond pulses with dense tissue. In our approach, we employed fluorescence labels to visualize photo damages occurring in deep-tissue. We propose the reported damage thresholds as the baseline, with higher damage threshold values anticipated for label-free nonlinear imaging. Furthermore, our study reveals that at peak intensities exceeding the CNS damage threshold, no discernible damage is evident at the epidermal level. This behavior can be associated with the four times lower photon flux on the skin compared to the spinal cord.

These findings significantly contribute to advancements of innovative microscopy techniques, including multi-modal microscopy [69, 70] or femtosecond fieldoscopy [66], by shedding light on the interaction of femtosecond pulses and deep-tissue. We not only lay down guidelines for emerging nonlinear imaging techniques but also suggest a strategy for inducing highly precise, deep-tissue, localized injuries, which is of interest for various research fields such as neuroregeneration [60, 71].

Methods

Irradiation and live imaging: An Yb:KGW amplifier (CARBIDE from Light Conversion) was used for irradiation of zebrafish. 20 μJ (on the microscope: from 3.75 pJ up to 14.2 nJ) of the output of the laser was frequency doubled in a 1.5 mm thick BBO crystal with 33.7° type I phase matching angle. A second BBO crystal was used for frequency tripling of the laser via cascaded second order effects [72]. The crystal was 1.5 mm thick with a phase matching angle of 62.8°, type II. Various beamsplitters were used to separate the fundamental beam from its harmonics at 515 nm and 343 nm. A reflective objective with a numerical aperture of 0.5 and a focal length of 5 mm (Thorlabs) was used to focus the beam to the zebrafish spinal cord. The beam size of the three beams were scaled to 3.5 mm to fill the 3.5 mm aperture of a reflective objective. The size of the beams at the focus were calculated using Abbe's resolution limit, resulting in beam sizes of 0.2 μm, 0.3 μm, and 0.6 μm for respective irradiation wavelength. The irradiation peak intensity was calculated based on these values. As the Rayleigh length of the focused beam is shorter than the transversal length of the samples, a camera is focused to ensure that the light is focused on the spinal cord. To calculate the peak intensity of the laser pulses on the skin of the zebrafish, it was assumed that the distance from the spinal cord to the skin of 3 dpf zebrafish is 100 μm. This information was used to calculate the beam size and the corresponding peak intensity of the irradiation beams on the skin. Live imaging after irradiation was done using a Plan-Apochromat 10x/0.45 M27 objective, or Plan-Apochromat 20x/0.8 objective on a Zeiss LSM 980 confocal microscope. For repetitive imaging, larvae were released from agarose after imaging, transferred to embryo medium at 28.5 °C, and re-mounted the following day.

Zebrafish husbandry and transgenic lines: All zebrafish lines were kept and raised under a 14/10h light-dark cycle as described according to FELASA recommendations [73, 74]. We used the following transgenic zebrafish lines: BAC(*pdgfrb*:Gal4ff)^{ncv24} [75], 5xUAS:EGFP^{zf82} [76], *mpeg1*:mCherry^{gl23} [77], *elavl3*:rasmKate2^{mpps1} [60], *her4.3*:GFP⁸³ [78] (formerly known as *her4.1*:GFP), and *krt1c19e*:EGFP^{sq1744} [79]. For all experiments, we used 3 day-old (dpf) zebrafish. Embryos were treated with 0.00375 % 1-phenyl-2-thiourea (Sigma-Aldrich #P7629) at 24 hpf to prevent pigmentation.

Zebrafish mounting: Zebrafish larvae were anesthetized in E3 medium containing 0.02 % Ethyl 3-aminobenzoate methanesulfonate (MS-222; PharmaQ #Tricaine PharmaQ) and mounted in a lateral position in 1 % low melting

point agarose (Ultra-Pure™ Low Melting Point, Invitrogen Cat#16520) between two microscope cover glasses. Larvae were covered with 0.01 % MS-222-containing E3 medium to keep preparations from drying out.

Whole-mount TUNEL labelling: Terminally anesthetized larvae were fixed in 4% PFA (Thermo Fisher Scientific Cat#28908) in PBS for overnight at 4°C. After removing the head and tail using micro scissors, larvae were permeabilized by subsequent incubation in acetone and Proteinase K (Invitrogen Cat#25530-049) as described elsewhere [80]. Samples were re-fixed in 4% PFA in PBS and Click-iT TUNEL Alexa Fluor 647 Imaging Assay (Thermo Fisher Cat#C10247) was performed according to the manufacturer's protocol to label apoptotic cells. Briefly, samples were equilibrated in TdT reaction buffer for 30 min at room temperature, followed by incubation in TdT reaction cocktail for overnight at room temperature. Samples were washed in PBTx and mounted in 75% glycerol in PBS. Imaging was done using a Plan-Apochromat 20x/0.8 objective on a Zeiss LSM 980 confocal microscope.

Acknowledgment

We thank Casandra Cecilia Carrillo Mendez and Olga Stelmakh for excellent fish care. H.F. acknowledges financial support from Max Planck Society. D.W. acknowledges financial support from the Deutsche Forschungsgemeinschaft (project number 460333672 – CRC 1540 Exploring Brain Mechanics (subproject B05)). S.J. acknowledges funding of the Erlangen Graduate School in Advanced Optical Technologies by the Bavarian State Ministry for Science and Art.

References

1. Talone, B *et al.* Phototoxicity induced in living HeLa cells by focused femtosecond laser pulses: a data-driven approach. *Biomedical Optics Express* **12**, 7886–7905 (2021).
2. Zhang, X., Dorlhiac, G., Landry, M. P. & Streets, A. Phototoxic effects of nonlinear optical microscopy on cell cycle, oxidative states, and gene expression. *Scientific Reports* **12**, 18796 (2022).
3. Wagner, M. *et al.* Light dose is a limiting factor to maintain cell viability in fluorescence microscopy and single molecule detection. *International journal of molecular sciences* **11**, 956–966 (2010).
4. Stelzer, E. H. Light-sheet fluorescence microscopy for quantitative biology. *Nature methods* **12**, 23–26 (2015).
5. Zhen, S., van Iersel, M. W. & Bugbee, B. Photosynthesis in sun and shade: the surprising importance of far-red photons. *New Phytologist* **236**, 538–546 (2022).
6. König, K, Becker, T., Fischer, P, Riemann, I & Halbhauer, K.-J. Pulse-length dependence of cellular response to intense near-infrared laser pulses in multiphoton microscopes. *Optics letters* **24**, 113–115 (1999).
7. Koester, H. J., Baur, D., Uhl, R. & Hell, S. W. Ca²⁺ Fluorescence Imaging with Pico- and Femtosecond Two-Photon Excitation: Signal and Photodamage. *Biophysical Journal* **77**, 2226–2236. ISSN: 0006-3495. <https://www.sciencedirect.com/science/article/pii/S0006349599770633> (1999).
8. König, K. Laser tweezers and multiphoton microscopes in life sciences. *Histochemistry and cell biology* **114**, 79–92 (2000).
9. Denk, W., Strickler, J. H. & Webb, W. W. Two-photon laser scanning fluorescence microscopy. *Science* **248**, 73–76 (1990).
10. Kerr, J. N. & Denk, W. Imaging in vivo: watching the brain in action. *Nature Reviews Neuroscience* **9**, 195–205 (2008).
11. Horton, N. G. *et al.* In vivo three-photon microscopy of subcortical structures within an intact mouse brain. *Nature photonics* **7**, 205–209 (2013).
12. Andresen, V. *et al.* Infrared multiphoton microscopy: subcellular-resolved deep tissue imaging. *Current Opinion in Biotechnology* **20**. Analytical biotechnology, 54–62. ISSN: 0958-1669. <https://www.sciencedirect.com/science/article/pii/S0958166909000214> (2009).
13. Velasco, M. G. M. *et al.* 3D super-resolution deep-tissue imaging in living mice. *Optica* **8**, 442–450. <https://opg.optica.org/optica/abstract.cfm?URI=optica-8-4-442> (2021).
14. Calovi, S., Soria, F. N. & Tønnesen, J. Super-resolution STED microscopy in live brain tissue. *Neurobiology of Disease* **156**, 105420. ISSN: 0969-9961. <https://www.sciencedirect.com/science/article/pii/S0969996121001698> (2021).
15. Helmchen, F. & Denk, W. Deep tissue two-photon microscopy. *Nature methods* **2**, 932–940 (2005).

16. Weigelin, B., Bakker, G.-J. & Friedl, P. Third harmonic generation microscopy of cells and tissue organization. *Journal of Cell Science* **129**, 245–255 (2016).
17. Squier, J. A., Müller, M., Brakenhoff, G. & Wilson, K. R. Third harmonic generation microscopy. *Optics express* **3**, 315–324 (1998).
18. Witte, S. *et al.* Label-free live brain imaging and targeted patching with third-harmonic generation microscopy. *Proceedings of the National Academy of Sciences* **108**, 5970–5975 (2011).
19. Debarre, D., Olivier, N., Supatto, W. & Beaurepaire, E. Mitigating Phototoxicity during Multiphoton Microscopy of Live Drosophila Embryos in the 1.0–1.2 μ m Wavelength Range. *PLoS One* **9**, e104250 (2014).
20. Ji, M. *et al.* Rapid, label-free detection of brain tumors with stimulated Raman scattering microscopy. *Science translational medicine* **5**, 201ra119–201ra119 (2013).
21. Müller, M., Squier, J., Wilson, K. & Brakenhoff, G. 3D microscopy of transparent objects using third-harmonic generation. *Journal of microscopy* **191**, 266–274 (1998).
22. Barad, Y., Eisenberg, H., Horowitz, M & Silberberg, Y. Nonlinear scanning laser microscopy by third harmonic generation. *Applied Physics Letters* **70**, 922–924 (1997).
23. Cheng, J.-X. & Xie, X. S. Coherent Anti-Stokes Raman Scattering Microscopy: Instrumentation, Theory, and Applications. *The Journal of Physical Chemistry B* **108**, 827–840. eprint: <https://doi.org/10.1021/jp035693v>. <https://doi.org/10.1021/jp035693v> (2004).
24. Tosheva, K. L., Yuan, Y., Pereira, P. M., Culley, S. & Henriques, R. Between life and death: strategies to reduce phototoxicity in super-resolution microscopy. *Journal of Physics D: Applied Physics* **53**, 163001 (2020).
25. Tirlapur, U. K., König, K., Peuckert, C., Krieg, R. & Halbhuber, K.-J. Femtosecond near-infrared laser pulses elicit generation of reactive oxygen species in mammalian cells leading to apoptosis-like death. *Experimental cell research* **263**, 88–97 (2001).
26. Khan, I., Tang, E. & Arany, P. Molecular pathway of near-infrared laser phototoxicity involves ATF-4 orchestrated ER stress. *Scientific Reports* **5**, 1–14 (2015).
27. Dillenburg, C. S., Almeida, L. O., Martins, M. D., Squarize, C. H. & Castilho, R. M. Laser phototherapy triggers the production of reactive oxygen species in oral epithelial cells without inducing DNA damage. *Journal of biomedical optics* **19**, 048002–048002 (2014).
28. Olivíe, G. *et al.* Wavelength dependence of femtosecond laser ablation threshold of corneal stroma. *Optics express* **16**, 4121–4129 (2008).
29. Sarpe-Tudoran, C., Assion, A., Wollenhaupt, M., Winter, M. & Baumert, T. Plasma dynamics of water breakdown at a water surface induced by femtosecond laser pulses. *Applied Physics Letters* **88**, 261109 (2006).
30. Astafiev, A. *et al.* Femtosecond Laser Microsurgery of Mouse Oocytes: Formation and Dynamics of Cavitation Bubbles Under the Action of Sharply Focused Laser Radiation on Various Oocyte Zones. *Russian Journal of Physical Chemistry B* **17**, 148–158 (2023).
31. Vogel, A., Noack, J., Huettmann, G. & Paltauf, G. *Femtosecond-laser-produced low-density plasmas in transparent biological media: a tool for the creation of chemical, thermal, and thermomechanical effects below the optical breakdown threshold in Commercial and Biomedical Applications of Ultrafast and Free-Electron Lasers* **4633** (2002), 23–37.
32. Laissue, P. P., Alghamdi, R. A., Tomancak, P., Reynaud, E. G. & Shroff, H. Assessing phototoxicity in live fluorescence imaging. *Nature methods* **14**, 657–661 (2017).
33. Wäldchen, S., Lehmann, J., Klein, T., Van De Linde, S. & Sauer, M. Light-induced cell damage in live-cell super-resolution microscopy. *Scientific reports* **5**, 1–12 (2015).
34. Linz, N., Freidank, S., Liang, X.-X. & Vogel, A. Wavelength dependence of femtosecond laser-induced breakdown in water and implications for laser surgery. *Physical Review B* **94**, 024113 (2016).
35. Hemmer, E., Benayas, A., Légaré, F. & Vetrone, F. Exploiting the biological windows: current perspectives on fluorescent bioprobes emitting above 1000 nm. *Nanoscale Horizons* **1**, 168–184 (2016).
36. Xu, W., Wang, D. & Tang, B. Z. NIR-II AIEgens: a win–win integration towards bioapplications. *Angewandte Chemie International Edition* **60**, 7476–7487 (2021).
37. Hong, G., Antaris, A. L. & Dai, H. Near-infrared fluorophores for biomedical imaging. *Nature biomedical engineering* **1**, 0010 (2017).

38. Smith, A. M., Mancini, M. C. & Nie, S. Second window for in vivo imaging. *Nature nanotechnology* **4**, 710–711 (2009).
39. Weissleder, R. A clearer vision for in vivo imaging. *Nature biotechnology* **19**, 316–317 (2001).
40. Olivier, N. *et al.* Cell lineage reconstruction of early zebrafish embryos using label-free nonlinear microscopy. *Science* **329**, 967–971 (2010).
41. Ferrer Ortas, J. *et al.* Label-free imaging of red blood cells and oxygenation with color third-order sum-frequency generation microscopy. *Light: Science & Applications* **12**, 29 (2023).
42. Sun, C.-K. *et al.* Higher harmonic generation microscopy for developmental biology. *Journal of structural biology* **147**, 19–30 (2004).
43. Oron, D. *et al.* Depth-resolved structural imaging by third-harmonic generation microscopy. *Journal of structural biology* **147**, 3–11 (2004).
44. Andresen, V. *et al.* Infrared multiphoton microscopy: subcellular-resolved deep tissue imaging. *Current opinion in biotechnology* **20**, 54–62 (2009).
45. Ouzounov, D. G. *et al.* In vivo three-photon imaging of activity of GCaMP6-labeled neurons deep in intact mouse brain. *Nature methods* **14**, 388–390 (2017).
46. Zhao, C. *et al.* Miniature three-photon microscopy maximized for scattered fluorescence collection. *Nature Methods*, 1–6 (2023).
47. Xu, Z. *et al.* Deep-brain three-photon imaging enabled by aggregation-induced emission luminogens with near-infrared-III excitation. *ACS nano* **16**, 6712–6724 (2022).
48. Grienberger, C., Giovannucci, A., Zeiger, W. & Portera-Cailliau, C. Two-photon calcium imaging of neuronal activity. *Nature Reviews Methods Primers* **2**, 67 (2022).
49. Streich, L. *et al.* High-resolution structural and functional deep brain imaging using adaptive optics three-photon microscopy. *Nature methods* **18**, 1253–1258 (2021).
50. Wang, T. *et al.* Quantitative analysis of 1300-nm three-photon calcium imaging in the mouse brain. *Elife* **9**, e53205 (2020).
51. Wu, W., Liu, Q., Brandt, C. & Tang, S. Dual-wavelength multimodal multiphoton microscope with SMA-based depth scanning. *Biomed. Opt. Express* **13**, 2754–2771. <https://opg.optica.org/boe/abstract.cfm?URI=boe-13-5-2754> (2022).
52. You, S. *et al.* Intravital imaging by simultaneous label-free autofluorescence-multiharmonic microscopy. *Nature communications* **9**, 2125 (2018).
53. Clark, M. G., Gonzalez, G. A. & Zhang, C. Pulse-Picking Multimodal Nonlinear Optical Microscopy. *Analytical Chemistry* **94**, 15405–15414 (2022).
54. Patel, K. B. *et al.* High-speed light-sheet microscopy for the in-situ acquisition of volumetric histological images of living tissue. *Nature Biomedical Engineering* **6**, 569–583 (2022).
55. Matsui, T. *et al.* Label-free multiphoton excitation imaging as a promising diagnostic tool for breast cancer. *Cancer Science* **113**, 2916 (2022).
56. Chen, I.-H., Chu, S.-W., Sun, C.-K., Cheng, P.-C. & Lin, B.-L. Wavelength dependent damage in biological multi-photon confocal microscopy: a micro-spectroscopic comparison between femtosecond Ti: sapphire and Cr: forsterite laser sources. *Optical and Quantum electronics* **34**, 1251–1266 (2002).
57. Magidson, V. & Khodjakov, A. in *Digital Microscopy* (eds Sluder, G. & Wolf, D. E.) 545–560 (Academic Press, 2013). <https://www.sciencedirect.com/science/article/pii/B9780124077614000233>.
58. Fu, Y., Wang, H., Shi, R. & Cheng, J.-X. Characterization of photodamage in coherent anti-Stokes Raman scattering microscopy. *Opt. Express* **14**, 3942–3951. <https://opg.optica.org/oe/abstract.cfm?URI=oe-14-9-3942> (2006).
59. He, H., Chan, K. T., Kong, S. K. & Lee, R. K. Y. Mechanism of oxidative stress generation in cells by localized near-infrared femtosecond laser excitation. *Applied Physics Letters* **95**, 233702 (2009).
60. Tsata, V. *et al.* A switch in pdgfrb+ cell-derived ECM composition prevents inhibitory scarring and promotes axon regeneration in the zebrafish spinal cord. *Developmental cell* **56**, 509–524 (2021).
61. Tsarouchas, T. *et al.* Dynamic control of proinflammatory cytokines *Il-1beta* and *Tnf-alpha* by macrophages in zebrafish spinal cord regeneration. *Nat Commun.* 2018; 9 (1): 4670 tech. rep. (Epub 2018/11/09. <https://doi.org/10.1038/s41467-018-07036-w> PMID: 30405119).

62. Mohanty, S., Rapp, A., Monajembashi, S., Gupta, P. & Greulich, K. Comet assay measurements of DNA damage in cells by laser microbeams and trapping beams with wavelengths spanning a range of 308 nm to 1064 nm. *Radiation research* **157**, 378–385 (2002).
63. Rapp, A. & Greulich, K. O. Why soft UV-A damages DNA: An optical micromanipulation study in *Optical Trapping and Optical Micromanipulation X* **8810** (2013), 162–169.
64. Curcio, J. A. & Petty, C. C. The Near Infrared Absorption Spectrum of Liquid Water. *J. Opt. Soc. Am.* **41**, 302–304. <https://opg.optica.org/abstract.cfm?URI=josa-41-5-302> (1951).
65. Fattahi, H. *et al.* Third-generation femtosecond technology. *Optica* **1**, 45–63 (2014).
66. Herbst, A. *et al.* Recent advances in petahertz electric field sampling. *Journal of Physics B: Atomic, Molecular and Optical Physics* (2022).
67. Kenry, Duan, Y. & Liu, B. Recent Advances of Optical Imaging in the Second Near-Infrared Window. *Advanced Materials* **30**, 1802394. eprint: <https://onlinelibrary.wiley.com/doi/pdf/10.1002/adma.201802394>. <https://onlinelibrary.wiley.com/doi/abs/10.1002/adma.201802394> (2018).
68. Golovynskiy, S. *et al.* Optical windows for head tissues in near-infrared and short-wave infrared regions: Approaching transcranial light applications. *Journal of Biophotonics* **11**, e201800141. eprint: <https://onlinelibrary.wiley.com/doi/pdf/10.1002/jbio.201800141>. <https://onlinelibrary.wiley.com/doi/abs/10.1002/jbio.201800141> (2018).
69. Francis, A. T. *et al.* In vivo simultaneous nonlinear absorption Raman and fluorescence (SNARF) imaging of mouse brain cortical structures. *Communications Biology* **5**, 222 (2022).
70. Guesmi, K. *et al.* Dual-color deep-tissue three-photon microscopy with a multiband infrared laser. *Light: Science & Applications* **7**, 12 (2018).
71. Matrone, G. *et al.* Laser-targeted ablation of the zebrafish embryonic ventricle: a novel model of cardiac injury and repair. *International journal of cardiology* **168**, 3913–3919 (2013).
72. Homann, C., Schriever, C., Baum, P. & Riedle, E. Octave wide tunable UV-pumped NOPA: pulses down to 20 fs at 0.5 MHz repetition rate. *Optics express* **16**, 5746–5756 (2008).
73. Brand, M & Granato, M. *Keeping and raising zebrafish. Zebrafish, a practical approach. Edited by: Nüsslein-Volhard C, Dahm R* 2002.
74. Aleström, P. *et al.* Zebrafish: Housing and husbandry recommendations. *Laboratory animals* **54**, 213–224 (2020).
75. Ando, K. *et al.* Clarification of mural cell coverage of vascular endothelial cells by live imaging of zebrafish. *Development* **143**, 1328–1339 (2016).
76. Asakawa, K. *et al.* Genetic dissection of neural circuits by Tol2 transposon-mediated Gal4 gene and enhancer trapping in zebrafish. *Proceedings of the National Academy of Sciences* **105**, 1255–1260 (2008).
77. Ellett, F., Pase, L., Hayman, J. W., Andrianopoulos, A. & Lieschke, G. J. mpeg1 promoter transgenes direct macrophage-lineage expression in zebrafish. *Blood, The Journal of the American Society of Hematology* **117**, e49–e56 (2011).
78. Yeo, S.-Y., Kim, M., Kim, H.-S., Huh, T.-L. & Chitnis, A. B. Fluorescent protein expression driven by her4 regulatory elements reveals the spatiotemporal pattern of Notch signaling in the nervous system of zebrafish embryos. *Developmental biology* **301**, 555–567 (2007).
79. Lee, R. T., Asharani, P. & Carney, T. J. Basal keratinocytes contribute to all strata of the adult zebrafish epidermis. *PloS one* **9**, e84858 (2014).
80. John, N., Kolb, J. & Wehner, D. Mechanical spinal cord transection in larval zebrafish and subsequent whole-mount histological processing. *STAR protocols* **3**, 101093 (2022).